Design Model of a Novel Cooling Condensation Type Atmospheric Water Generator for Coastal Rural South Africa

S. Thisani, D. V. V. Kallon and E. Bakaya-Kyahurwa

Department of Mechanical and Industrial Engineering Technology,
University of Johannesburg

Abstract

In many of South Africa's rural communities, rivers and rain water storage tanks are the main source for domestic water supply and agricultural use. However, from 2015 to date South Africa has faced severe water shortages due to the worst droughts the country has experienced in over 23 years. The droughts have led to the reduction in flow volumes of some rivers and domestic rain water storage tanks being rendered mostly empty. This greatly endangered the livelihoods of many rural communities in South Africa. This study investigates the implementation of an affordable cooling condensation type Atmospheric Water Generator (AWG) solution for coastal rural households as a supplementary water source in the event of water crisis. The eastern coastal region of KwaZulu-Natal (KZN), situated between the towns of Amanzimtoti and St. Lucia, was chosen as the case study location due to the favourable climate conditions for the implementation of AWG technology as well as the large number of surrounding rural communities that have been affected by the on-going draughts. An accumulation of 10 litres of water over a period of 10 hours was defined as the minimum requirement for water production. Based on this target concept, a detailed AWG design was developed. A computational fluid dynamics (CFD) simulation was implemented to predict the performance of the system. The study found that for ambient air temperatures of 21˚C or higher and relative humidity of 65% or higher, a cooling condensation type AWG device can be a feasible alternative water supply solution for domestic use in South African rural communities. The development of a new model cooling condensation AWG and its analysis forms the focus of this paper.

Key words: Computation Fluid Dynamics (CFD), Atmospheric Water Generator (AWG), Humidity, Evaporator.

Corresponding Author emails: dkallon@uj.ac.za
Sandisiwe.Thisani@gmail.com

Nomenclature

A	=	Area	[m^2]
COP	=	Coefficient of performance	[-]
D	=	Diameter	[m]
h_{tp}	=	Two phase convective heat transfer coefficient	[W/ m2 ·K]
h_a	=	Enthalpy of air	[kJ/kg]
h_{fg}	=	Enthalpy of vaporization	[kJ/kg]
K	=	Conduction heat transfer co-efficient	[W/m·K]
L	=	Length of tube	[m]
$\dot{m}_a$	=	Mass flow of humid air	[kg/s]
$\dot{m}_w$	=	Mass flow of water vapour	[kg/s]
M_w	=	Mass of condensed water	[kg]
P	=	Pressure	[kPa]
P_g	=	Total pressure of the air and vapour mixture	[kPa]
P_S	=	Saturation pressure of water vapour	[kPa]
P_T	=	Total pressure / ambient atmospheric pressure	[kPa]
Q	=	Rate of heat transfer	[kW]
r_{LM}	=	Log mean radius	[m]
T_∞	=	Ambient air temperature	[˚C]
β	=	Bypass factor	[-]
ω	=	Humidity ratio	[kg/kg]
∅	=	Relative humidity	[%]

1. Introduction

Rural households in South Africa depend heavily on rain and river water for fulfilling their basic needs. From 2015 to date South Africa has been faced with severe water shortages due to the worst droughts the country has experienced in over 23 years. The efforts of the South African government to alleviate this water crisis is hampered by a lack of an alternative water source to supply water to rural homes. This necessitated the development of an alternative water supply solution suited to the unique climate and socio-economic constraints of South African rural households. In this paper, a computational model of an AWG is developed and the performance simulated using CFD.

The aim of this study is to determine whether a cooling condensation type AWG could be used as a partial solution for the current water crisis in South Africa specifically in coastal rural households.

The atmosphere contains large volumes of water in the form of moisture or water vapour which can be quantified by the humidity ratio. It is a well-known fact that at higher ambient temperatures and relative humidity the moisture content in air increases proportionally. AWG technology can be used to retrieve the water vapour by drawing large volumes of moist air from the environment and displacing it across a heat exchanging element which causes the moist air to cool down to below its dew point temperature and the water vapour to condense to liquid.

2. Literature Review

The Council of Science and Industrial Research (CSIR, 2011) conducted a study on the patterns of average moisture content over southern Africa from 1901 to 2009 and found that below the equatorial region there is an increasing gradient in the relative humidity from the west to the east due to the moisture from the Indian Ocean. Consequently, the KZN area, located on the far eastern region of South Africa, is the most humid area in the country. The mean annual relative humidity in the case study location from 1901 to 2009 is in the range of 60 – 70% (CSIR, 2011).

South African Statistics (2005) published the average maximum and minimum temperatures for the major South African cities over the period of 1961 to 2003 (South African Statistics, 2005). According to this publication the average annual mean temperature experienced in the case study location over the period of 1961 to 2003 is 20.85°C. The average extreme high temperature experienced over the period is 35.5°C. The South African Department of Environmental Affairs (2013) and MacKellar et al. (2014) published reports on climate trends observed in South Africa from 1960 to 2010. In their studies the researchers projected the change in temperatures which can be expected in all regions of South Africa for the next 80 years. The forecasts of the change in the temperature of South African hydrological zone 2, the coastal region of KZN where the case study is located, show a significant mean increase in the annual minimum and maximum temperature; a steady increase in the number of days annually with maximum temperature above the 90^{th} percentile of the daily maximum temperature and a slight decrease in the number of days annually with minimum temperature below the 10^{th} percentile of the daily minimum temperature (Department of Environmental Affairs RSA, 2013; MacKellar, et al., 2014).

Three climate conditions are identified to test the performance of the design developed in this paper, namely; the worst case operation climate conditions for efficient water production of existing AWG solutions; the average historic climate data in the case study location; and the extreme high conditions in the case study location based on historic climate data. The three operating conditions identified for this design are as defined in Table 1.

Table 1: Operating climate conditions

Condition	Lowest Operating Point	Mean Operating Point	Optimum Operating Point
Relative Humidity (Ø)	40%	65%	80%
Ambient Temperature (T_∞)	15 ˚C	21 ˚C	35 ˚C
Dew Point (T_{DEW})	5 ˚C	14 ˚C	34 ˚C
Enthalpy (h)	25.9 kJ/kg	47.06 kJ/kg	110.6 kJ/kg

A cooling condensation type AWG uses refrigeration technology to condense water vapour and produce water. The cooling condensation type AWG is the most commonly available AWG solution on the market (Bruce, et al., 2008; Niewenhuis, et al., 2012). This AWG system typically consists of a refrigerant compressor, an evaporator, a condenser, a high-performance air filter to remove up to 99.9% of particles in air as small as 0.3µm (Filt Air Ltd., 2014; Cambridge Filter Corporation, 2006), water storage capabilities and can also include a water purification system.

The compressor pumps refrigerant through the system. The refrigerant pressure increases proportionally to the refrigerant temperature. The compressor discharges the refrigerant as a superheated vapour (Bruce, et al., 2008). The high pressure and high temperature refrigerant vapour releases heat to the surroundings. As the refrigerant vapour loses heat it condenses and becomes a sub-cooled high pressure liquid (Bruce, et al., 2008). The component in which the refrigerant vapour condenses to a sub-cooled high pressure liquid is known as the condenser. The sub-cooled high pressure liquid refrigerant then passes through an expansion valve which reduces the pressure of the refrigerant. Due to the pressure drop the refrigerant experiences a temperature drop. The refrigerant flashes to a low pressure liquid-vapour mixture after passing through the expansion valve (da Cunha, 2010). The low temperature liquid-vapour refrigerant then goes through the evaporator and absorbs heat from the surroundings; in the case of an AWG the heat absorbed is mainly from the humid air (Bruce, et al., 2008). The absorption of heat leads to the evaporation of the liquid refrigerant to a low pressure superheated vapour (da Cunha, 2010; Niewenhuis, et al., 2012). The low pressure vapour flows to the suction of the compressor and the cycle is repeated. During this process the humid air is cooled down to below its dew point temperature at which the water vapour condenses and is collected in a reservoir.

Figure 1 is a schematic illustration of the operation of a cooling condensation type AWG.

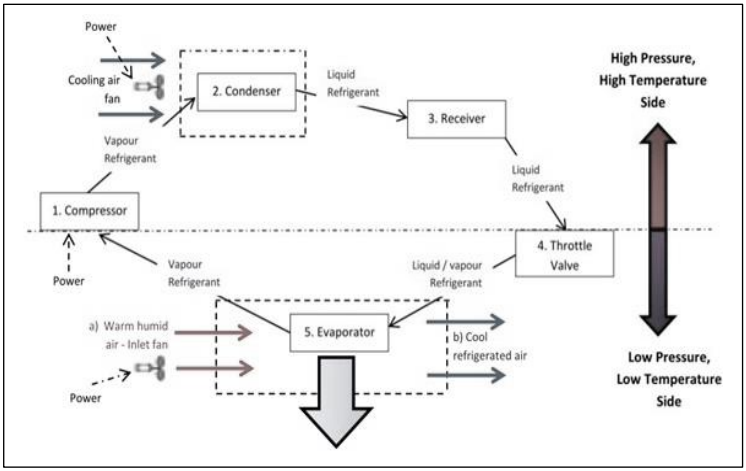

Figure 1: Condensation cycle of a cooling condensation type AWG

3. Methodology

In this study data is obtained from various existing weather statistics and compounded with data obtained using a numerical simulation approach. The evaporator is responsible for cooling the moist air to below the dew point temperature and therefore this component is the key focus of this paper. The design model is developed from first principal steady state heat transfer calculations. A three-dimensional Computer Aided Drawing (CAD) model of the AWG design is developed from the results of the first principal calculations. The design model is computationally simulated to predict the performance of the design. The simulations are conducted in the Autodesk CFD 2017 software. The performance outcomes of the design model are analysed to determine the feasibility of implementing this design as an emergency water source in South African rural households in the event of a water crisis.

The atmospheric conditions in the case study location are defined based on historical weather patterns and projected future climate conditions. The three climate conditions identified to test the performance of the AWG device are as defined in Table 1.

4. Model Development

When air is blown over the evaporator coils during operation of the AWG, a portion of the air volume does not come into contact with the coils. This portion of the air volume flows in between the coils and is not directly cooled by the evaporator surface. The air stream in contact with the coils is cooled down to the temperature of the external surface of the coils and reaches saturation at this temperature. For this reason the temperature of the coil surface is commonly referred to as the Apparatus Dew Point (ADP). The air stream which does not come into contact with the coils is cooled indirectly by mixing with the cooled air. The percentage of air volume which is not cooled down to the ADP is known as the bypass factor. The bypass factor is also used as an indicator of the heat exchangers efficiency. Figure 2 illustrates the bypass factor concept.

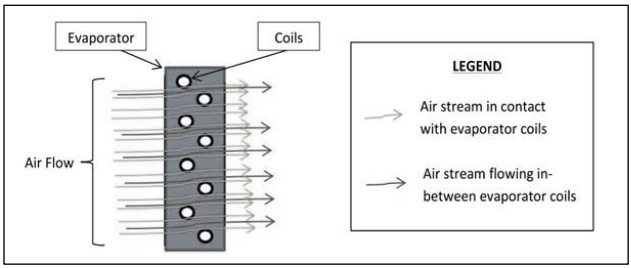

Figure 2: Typical flow path of air over heat exchanger coils

Figure 3 illustrates the cooling dehumidification process of air on a graphical representation of a psychometric chart. The process illustrated in this figure is explained as follows:

- 1 – 2: The air stream which comes into contact with the evaporator is cooled to its saturation.
- 2 - 3: The saturated air is further cooled to the APD. During this process air is dehumidified.

- 3 - 4: The air stream which bypasses the evaporator coils mixes with the cooled air which has made contact with the coils. The mixing results in re-humidification of the saturated air while it increases the temperature of the saturated air. State 4 is then the final condition of the bulk air as it exits the evaporator.

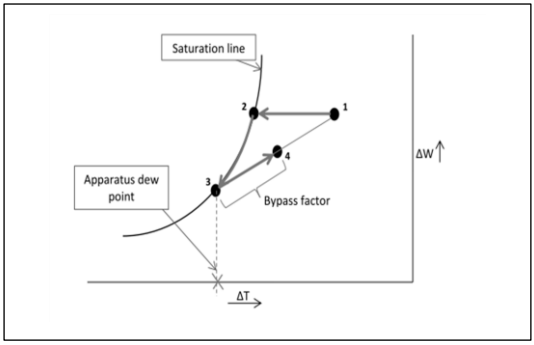

Figure 3: Cooling dehumidification process of air on graphical representation of a psychometric chart

The initial states for the three operating conditions are as defined in Table 1. The final state of the worst case duty point is designed to initially be as close to the ADP as possible for maximum water vapour condensation.

To produce 10 litres of water in 10 hours the required mass flow rate of water is:

$$\dot{m}_w = \frac{10kg}{10\ (hours) \times 60\ (minutes) \times 60\ (seconds)} \qquad (1)$$

$$\dot{m}_w = 0.000278kg/s$$

The humidity ratio can be defined as the ratio between the mass of water vapour present in air to the mass of the air. The humidity ratio for the initial and final states of the three case scenarios are determined using Equation 2.

$$\omega_i = 0.622 \times \frac{P_g \emptyset}{P_T - (P_g \emptyset)} \quad (2)$$

The values of P_S and P_g are obtained from psychometric tables at the specific air conditions. The mass flow of air required to produce the 10 litres of water in 10 hours is obtained from Equation 3.

$$\dot{m}_a = \frac{\dot{m}_w}{(\omega_1 - \omega_2)} \quad (3)$$

$$\dot{m}_a = \frac{0.000278}{(0.0042 - 0.0016)}$$

$$\dot{m}_a = 0.107 kg/s$$

The initial (i =1) and final (i = 2) humidity ratios of the air at the worst case scenario are plotted on a psychometric chart to obtain the enthalpy of the two states. Change in enthalpy is then used to determine the cooling energy required to change the sensible and latent heat of the air such that the ADP is reached. The cooling load is determined from Equation 4.

$$Q_{COOLING} = \dot{m}_a [h_{a_1} - h_{a_2}] \quad (4)$$

$$Q_{EVAP} = 0.107 [25.9 - -6.065]$$

$$Q_{EVAP} = 3.42 kW$$

For the mean and optimum operating conditions the final state of the air is determined by reversing Equation 4 and making the final enthalpy the unknown variable.

Table **2** 2 show the initial and final states of air for the three operating conditions as well as the water produced and bypass factors at the three operating conditions as determined from the steady state calculations.

Table 2: Initial and final operating points of moist air

Condition	Lowest Operating Point		Mean Operating Point		Optimum Operating Point	
	Initial State	Final State	Initial State	Final State	Initial State	Final State
Relative Humidity (Ø)	0.4	1	0.65	1	0.8	0.96
Bulk Temperature	15°C	-10°C *	21°C	2.5°C	35°C	26°C
Bypass factor (β)	100% *		59.68%		20%	
Saturation pressure of air and vapour mixture (P_g)	1.7kPa	0kPa	2.49kPa	0.73kPa	5.62kPa	3.17kPa
Saturation pressure of the water vapour (P_s)	0.6kPa	0kPa	1.494kPa	0.735Pa	4.496kPa	3.043kPa
Total pressure (P_T)	101.3kPa	101.3kPa	101.3kPa	101.3kPa	101.3kPa	101.3kPa
Humidity Ratio – kg of water per kg of dry air (ω)	0.0042kg/ kg	0.0016kg /kg	0.0101kg/ kg	0.0045kg/ kg	0.0289kg /kg	0.0193kg/ kg
Water Production in 10 hours	10 litres		21.38 litres		37.11 litres	

*Specified conditions for optimum performance.

The cooling capacity of the evaporator needs to be higher than the required cooling load to condense the moist air to its final state due to the foreseen bypass and design inefficiencies. To account for these inefficiencies a 15% factor is added to the cooling load required thus defining the cooling capacity of the evaporator as:

$$Q_{EVAP} = 3.42 \times (1 + 0.15) \quad (5)$$

$$Q_{EVAP} = 3.933kW$$

The refrigerant chosen for this design is R-134a due to its good performance characteristics, non-toxicity, non-flammability and zero ozone depletion potential (Matsunaga, 2002). The properties of the refrigerant entering the evaporator in this design are 25% quality; temperature of -10°C; pressure of 0.2MPa and enthalpy of 240kJ/kg. The properties of the refrigerant leaving the evaporator is initially set as a -5°C superheated vapour at 390kJ/kg. The required mass flow of refrigerant through the evaporator is determined using Equation 6.

$$Q_{EVAP} = \dot{m}_{R-134a}(h_2 - h_1) \quad (6)$$

$$3.933 = \dot{m}_{R-134a}(390 - 240)$$

$$\dot{m}_{R-134a} = 0.02611 kg/s$$

The design of this evaporator is based on a finned tube type model. The surface area, spacing between fins, geometry and number of fins on the evaporator are influential parameters on the overall cooling efficiency of the evaporator. The rate of heat transfer across the tube surface area is a function of the convection of heat by the refrigerant inside the tube; the conduction of the heat through the thickness of the tube material and the forced convection of air over the tube surface. The rate of heat transfer across the fin surface area is a function of conduction from the tube through the fin surface area and the forced convection of air over the fin surface. Equations 7 and 8 are used to define the rate of heat transfer across the tube and the fin respectively to determine the required surface area.

$$Q_{TUBE} = \frac{T_\infty - T_1}{\frac{1}{h_{tp}(\pi D_i L)} + \frac{1}{2\pi LK}\frac{(r_o - r_i)}{r_{LM}} + \frac{1}{h_o(\pi D_o L)}} \quad (7)$$

$$Q_{FIN} = \sqrt{hPKA_c} \times [T_b - T_\infty]\tanh[mL] \quad (8)$$

From these Equations the design parameters of the evaporator are determined as shown in Table 3.

Table 3: Design parameters of evaporator

	Description	Design Parameter
1	Evaporator type	Finned tube type
2	Tube specifications	5 meters long 10NB (3/8”), Type L copper tube,
3	Fin specifications	5 mm thick, aluminium fin
4	Required mass flow of air	0.107 kg/s
5	Required mass flow of refrigerant	0.02611 kg/s

The refrigeration system is designed with a Coefficient of Performance (COP) of 3.5 based on the optimum COP of existing refrigeration systems using R-134a (Domanksi, 1995). Each stream of the refrigeration cycle is determined as illustrated in Table 4 and Figure 4.

Table 4: Properties of the refrigerant at each stage of the vapour compression cycle

Stream	State	Pressure [P]	Enthalpy [h]	Entropy [s]	Temp. [T]
1	25% vapour 75% liquid	200.6kPa	240kJ/kg	1.00kJ/kg·K	-10˚C
1a	Saturated vapour	200.6kPa	385kJ/kg	1.733kJ/kg·K	-10 ˚C
2	Superheated vapour	200.6kPa	390kJ/kg	1.75kJ/kg·K	-5 ˚C
3	Superheated vapour	1421kPa	433kJ/kg	1.75kJ/kg·K	66 ˚C
3a	Saturated vapour	1421kPa	422kJ/kg	1.715kJ/kg·K	53˚C
4	Sub-cooled liquid	1421kPa	240kJ/kg	1.00kJ/kg·K	30˚C

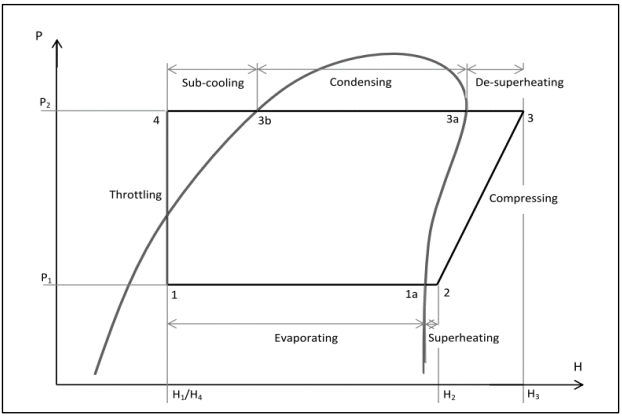

Figure 4: Labelled pressure vs. enthalpy chart for this design's vapour compression cycle

The main energy consumer in this design is the refrigerant compressor. The energy consumed by the evaporator fan is negligible in comparison to the compressor's power requirements. A compressor efficiency of 80% is used in this design based on refrigerant compressor efficiencies of existing systems (Reddy, et al., 2013). The power absorbed by the compressor is determined using Equation 9 with the variables defined in Table 4.

$$W_{COMP} = \dot{m}_{R-134a}\,[h_3 - h_2] \times {}^{1}/_{\eta} \qquad (9)$$

$$W_{COMP} = 0.026\,[433 - 390] \times {}^{1}/_{0.8}$$

$$W_{COMP} = 1.408kW$$

Figure 5 and 6 illustrate the process flow diagram and the general arrangement of the design model developed in this study respectively.

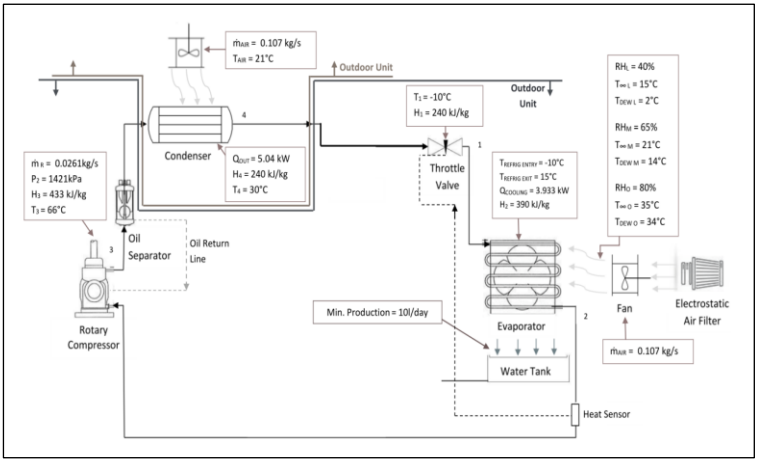

Figure 5: Process flow diagram

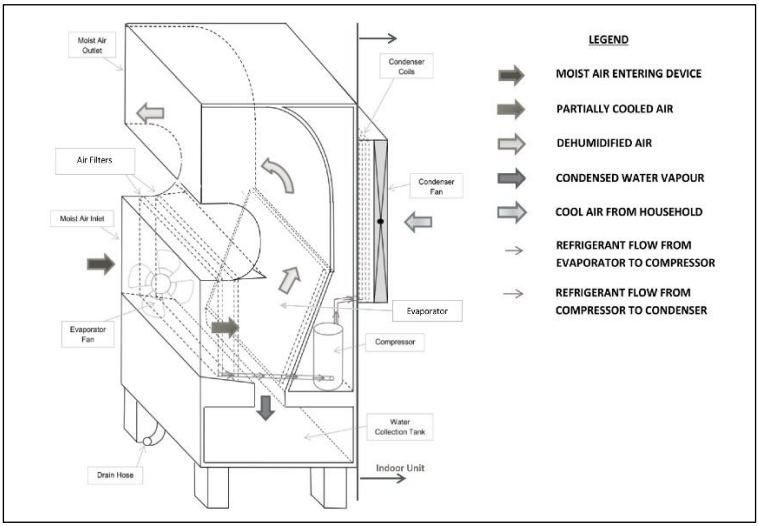

Figure 6: General arrangement of design model

5. Simulation Results

5.1 CAD and CFD modelling

Figure 7 illustrates the evaporator CAD model developed from the design calculations. The refrigerant is fed though the centre of the evaporator and exits the evaporator as a superheated vapour.

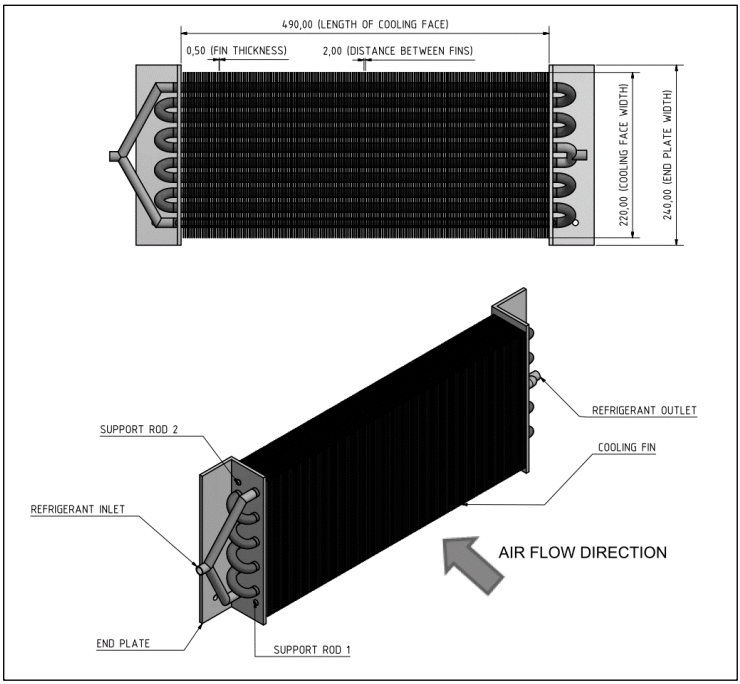

Figure 7: Evaporator model

The inputs to the CFD software for the simulation of the evaporator model are summarised in Table 5.

Table 5: CFD input parameters for preliminary evaporator model

MATERIALS			
1	Cooling Fins	Aluminium 6061	
2	Tube	Copper	
3	Support Rods	Stainless Steel 316	
4	Fluid Moving Over Cooling Surface	Scenario 1: Air (15°C at 40% RH) Scenario 2: Air (21°C at 65% RH) Scenario 3: Air (35°C at 85% RH)	
5	Fluid Moving Inside of Tube	R-134a (Two phase, 25% vapour and 75% liquid)	
6	Fluid Travelling across evaporator cooling surface	Moist air	
6	External Surface Material Insulating Air Flow	ABS Plastic	
7	End Plate	300WA Carbon Steel (Coated)	
BOUNDARY CONDITIONS			
	Surface	**Condition Type**	**Specified Condition**
8	Refrigerant Inlet	Temperature	-10°C
9	Refrigerant Inlet	Mass flow	0.0261 kg/s
10	Refrigerant Outlet	Pressure	0 kPa (exit condition)
11	Air Inlet	Temperature	Scenario 1: 15°C Scenario 2: 21°C Scenario 3: 35°C
12	Air Inlet	Mass flow	0.107 kg/s
13	Air Inlet	Humidity	Scenario 1: 40% Scenario 2: 65% Scenario 3: 85%
14	Air Outlet	Pressure	0 kPa (exit condition)
MESH SIZING			
	Description	**Selected Function**	**Details**
15	Surface and Volume Mesh	Automatic Fine Mesh Setting; 3 layers, 0.3 layer factor	2814140 Nodes; 10251643 elements
SOLVING			
16	Solver Physics	Solve for incompressible flow, heat transfer, auto forced convection,	

Figure 8 shows the air stream flow vectors across the evaporator. The flow streams are laminar with no choked zones which prevents high pressure drop across the evaporator and promotes energy efficiency.

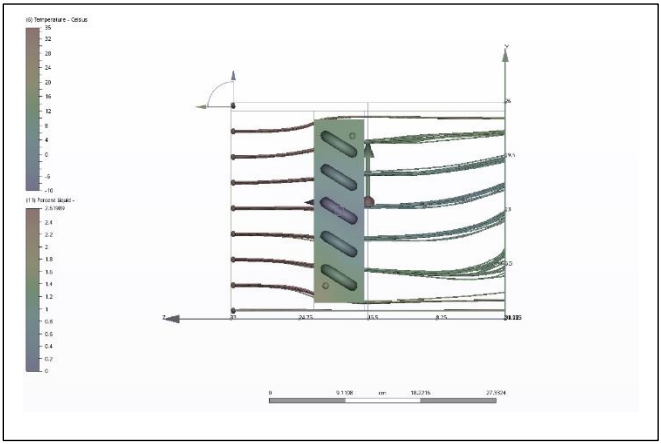

Figure 8: Air flow vectors across evaporator

5.2 Scenario 1: CFD Results

Figure 9 illustrates the formation of saturated water vapour across the evaporator at the worst case condition. The water vapour saturates over the central portion of the evaporator which is approximately one third of the surface area. The cooling capacity of the evaporator is insufficient to cool the air below the dew point temperature over the full surface area of the evaporator. To increase the cooling capacity a higher mass flow rate of refrigerant is required which results in additional operational cost due to more energy required to drive the compressor and higher capital costs due to a bigger compressor required as well as a great volume of refrigerant required. The bulk average temperature of the air exiting the evaporator is 5°C. The average bulk temperature of the condensed water vapour is -1°C at a relative humidity of 75%. To determine the amount of water condensed the final state of the saturated water vapour is plotted on a psychometric chart**.** The percentage liquid (a measure of the rate of condensation from 0 being no condensation

taking place and 1 water vapour condensing to liquid continuously) for the worst case operating condition is 0.242 which indicates a very low rate of condensation.

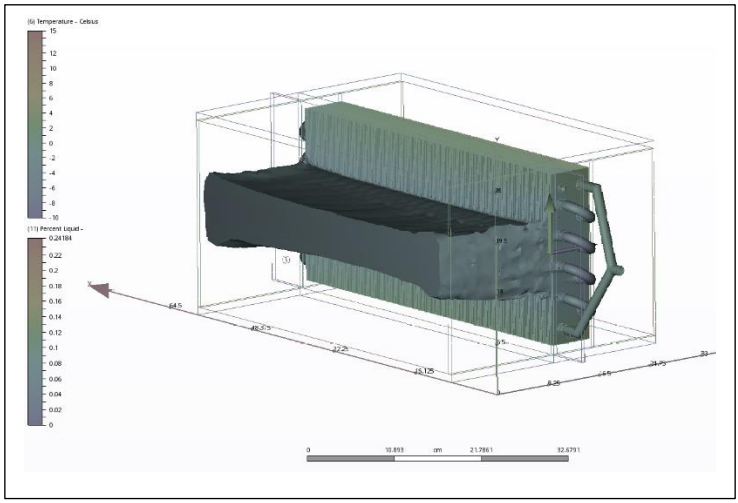

Figure 9: Condensation formation for worst case operating conditions

5.3 Scenario 2 Results

Figure 10 shows the fully developed condensation of water vapour over the entire surface area of the evaporator at the mean operating condition. The bulk temperature of the air and water vapour mixture exiting the evaporator is 6.4°C. The bulk relative humidity of the air exiting the evaporator is 100%. The percentage liquid for the optimum operating condition is 0.8 which indicates a moderate rate of condensation across the evaporator. The performance of the system is improved at the mean condition with condensation taking place over the full surface area of the evaporator at a high percentage of liquid.

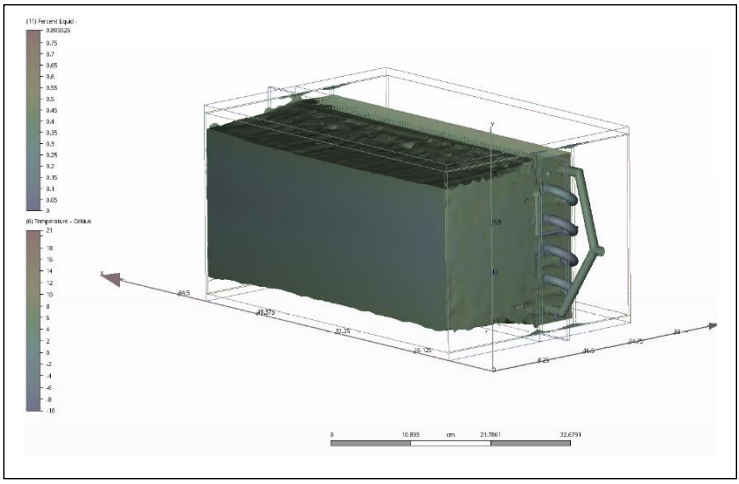

Figure 10: Condensation formation for mean operating conditions

5.4 Scenario 3 Results

Figure 11 shows the fully developed condensation of water vapour over the entire surface area of the evaporator at the optimum operating condition. The bulk temperature of the air and saturated water vapour exiting the evaporator is 20°C. The bulk relative humidity of the air exiting the evaporator is 100%. The water production of the system is significantly improved at the optimum condition with condensation taking place over 100% of the evaporator surface area at a high percentage of liquid. The bypass ratio is considerably lower for scenario 3 with the bulk temperature exiting the evaporator 30°C higher than the ADP.

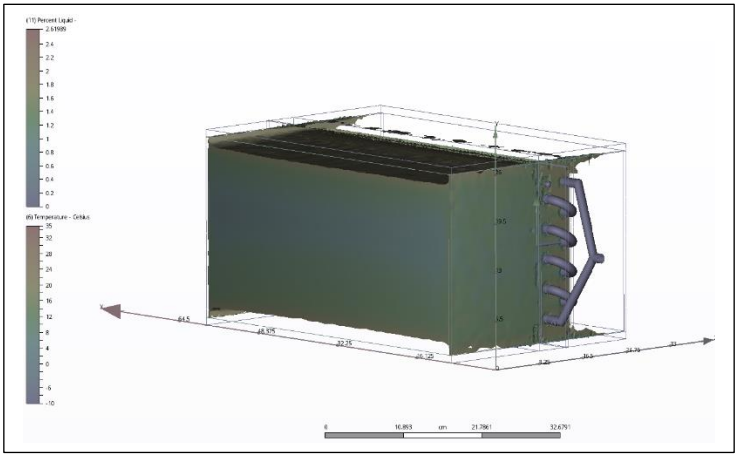

Figure 11: Condensation formation for optimum operating conditions

5.5 Combined Results

5.5.1 Water production

The results obtained from the CFD analysis are plotted on a psychometric chart to determine the water condensed by the AWG design. Table 6.

Table **6** show the initial and final states of the moist air at the three operating conditions as defined by the CFD analysis. The amount of water produced is a function of the difference in the initial and final state humidity ratio. Equation 10 is used to determine amount of water produced based on the psychometric chart readings.

$$M_W = \dot{m}_a(\omega_1 - \omega_2) \times t \qquad (10)$$

To determine the quantity of water produced for the first scenario one third of the mass flow of air is used in Equation 10 due to only one third of the air being cooled to the saturation point as illustrated on Figure 9. For scenario 2 and 3 the full mass flow is used to determine the amount of water condensed due to the condensation

taking place over the full surface area of the evaporator in these two scenarios. The amount of water produced is given on Table 6.

Table 6: Initial and Final Operating Points of Moist Air as Determined from CFD Analysis

Condition	Lowest Operating Point		Mean Operating Point		Optimum Operating Point	
	Initial State	Final State	Initial State	Final State	Initial State	Final State
Relative Humidity (Ø)	0.4	0.75	0.65	1	0.8	1
Temperature [T]	15°C	-1°C	21°C	6°C	35°C	20°C
Humidity Ratio – kg of water per kg of dry air (ω)	0.0042kg/ kg	0.0024kg/ kg	0.0101kg/ kg	0.006kg/k g	0.0289kg/ kg	0.0148kg/ kg
Amount of water produced [M_W]	2.311 litres		15.79 litres		54.3 litres	

5.5.2 Comparison of calculation and simulation results

Table 7 shows a comparison of the calculated and simulated results for the performance of the AWG design.

Table 7: Calculation and simulation results

	Scenario 1		Scenario 2		Scenario 3	
Parameters	Calculated	Simulated	Calculated	Simulated	Calculated	Simulated
Exit Temperature	-10°C*	-1°C**	2.5°C	6.4°C	26°C	20°C
Bypass factor	100%*	64%	59.68%	47.1%	20%	33.33%
Water Production	10 liters	2.31 liters	21.38 liters	15.79 liters	37.11 liters	54.3 liters

*Specified conditions for optimum performance.

**Temperature of saturated water vapour

The major difference between the calculated and simulated results is the bypass factors. Figure 13 and 14 show graphical comparisons of the calculated and simulated results.

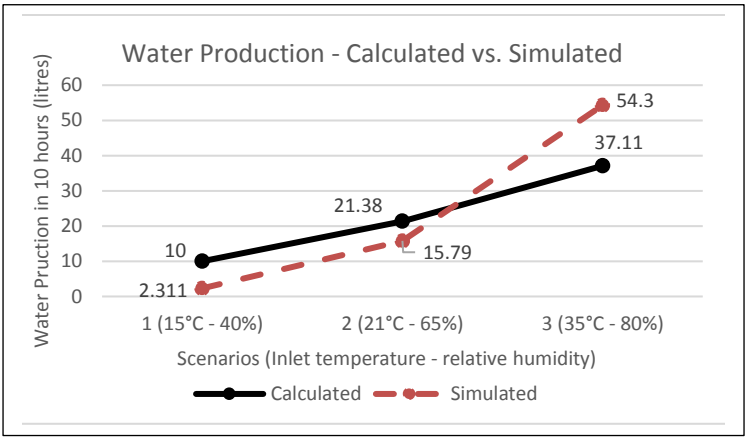

Figure 12: Water production – calculated vs. simulated graph

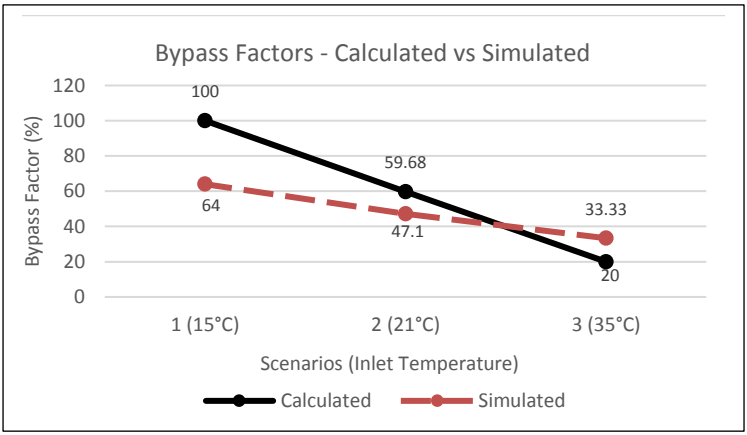

Figure 13: Bypass factor - calculated vs. simulated graph

From Figure 12 and 13 it can be seen that an increase in the inlet temperature and relative humidity leads to an increase in the water production while the bypass factor decreases proportionally. The average variance between the calculated and simulated bypass factor is 20% while the average variance between the calculated and

simulated water production is 10.15 litres. The degree of variation in the water production results due to the bypass factor is significant. This illustrates that optimisation of the bypass factor can yield large water production improvements. The degree of variance in the two sets of results is due to geometric, dimensional and flow properties which cannot be accounted for accurately in first principal methods.

5.5.3 Cost and energy consumption

From Equation 9 it was determined that the compressor consumes approximately 1.408kWh. The power consumed by the fan is negligible in comparison to the compressor's power demand. The operating duration is 10 hours per day therefore the AWG consumes 14.08kW/day. The cost of three phase electricity in Ethekwini Municipality, the central municipality to the case study location, in 2016 was R1.29 per kWh (Ethekwini Municipality, 2015). The cost of water in Ethekwini Municipality for the lowest consumption bracket of less than 25 kilolitres of water per month was R9.20 per kilo litre in 2016 (Ethekwini Water and Sanitation, 2015). Table 8 defines the energy consumed to produce a litre of water, the cost per litre of water produced as well as the cost per kilo litre of water produced at each of the three scenarios. Table 8 uses the results obtained from the CFD simulations due to the higher degree of accuracy in predicting the performance of the system.

Table 8: Power Consumed and Operational Costs for Producing Water

	Scenario 1	**Scenario 2**	**Scenario 3**
Litres produced in 10 hours	2.3 l	15.79 l	54.3 l
Energy consumed per litre	6.12kW	0.89kW	0.26kW
Cost per litre	R 7.90	R 1.15	R 0.34
Cost per kilolitre	R7900	R1150	R340

6. Discussions

The bypass factor is an influential parameter in the performance of an AWG evaporator. The findings in this study show inverse proportionality between the bypass factor and the inlet air temperature for both the calculated and simulated conditions. The bypass factor is thus seen as a function of various parameters which include air flow, number of tube rows, spacing between fins, fin profile, cooling area and refrigerant flow (Paranjpey, 2003). These factors cannot be accounted for entirely from first principal calculations therefore first principal methods cannot be used to accurately predict AWG performance.

The CFD analysis shows that at the lowest case condition the requirement of 10 litres in 10 hours is not obtained with this design. Additionally, the water vapour is saturating at -1°C and this leads to a high possibility of frost build-up over the coils which can result in reduced heat transfer efficiency. The cost per litre produced at the worst case scenario is over 850 times more expensive than the municipal tariff. Findings in this study suggest that operating a cooling condensation type AWG at 40% relative humidity or lower and a temperature of 15°C or lower is highly inefficient and uneconomical.

At the mean operating condition the minimum requirement of water production is exceeded. The water vapour saturates at 6°C, therefore there is only a very moderate to negligible risk of frost build-up and the AWG device can be operate continuously The cost of water (per litre) produced by the design is considerably lower than purchasing bottled water which ranges from R5.00 to R8.00 per litre. However, the cost of producing water at the mean condition is 125 times more expensive than the municipal tariff. In the event of a water crisis rural households can gain financial benefit from using this AWG solution at the mean condition as they would save considerably on

travel costs to the nearest town as well as costs to purchase expensive bottled water.

At the optimum operating condition the minimum requirement of water production is well exceeded. At this condition water can be produced at a cost of 100 times less than the purchasing price of bottled water. Although the cost of producing water with this AWG design is still more expensive than the municipal tariff, the volumes produced at this condition are large enough to satisfy the basic needs of a household at a reasonable cost. This optimum condition occurs only in summer and spring and is infrequent therefore its results are not considered as influential findings for this study.

7. Conclusions

The use of an AWG in coastal rural households should be considered as an alternative water source in the coastal KZN region of the country for water crisis relief. Although the solution was found to be inefficient at low relative humidity and temperature in this study, the probability for suitable climate conditions in the KZN region is high with the annual average relative humidity and temperature being a favourable 65% and 21°C respectively over the past five decades. The costs of operating the system at the mean condition is considerably lower than purchasing bottled water which gives financial benefit in water crisis situations.

The capital expenditure (CAPEX) to build this system as well as the maintenance required on the device are key determinants in the feasibility of this solution and need to be considered for an overall understanding of this solution. From an operational costs perspective there can be benefits in implementing the solution in emergency situations.

This study broadens the knowledge on the overall capabilities and limitations of AWG technology. For further studies it is recommended that a model of the design is built and tested. It is further recommended that a financial model which includes the CAPEX and maintenance costs of the design is developed to definitively define the feasibility of AWG technology as a water crisis relief solutions for coastal KZN communities.

8. Acknowledgements

We would like to acknowledge and thank the National Research Foundation (NRF) of South Africa for their partial funding of this project.

9. Bibliography

Bruce, H., Brannstromm, E., Dahlbeck, E. & et.al, 2008. *Mimer: Winter Quarter Report - Atmospheric Water Generator.* Immerse Global(California): Department of Mechanical Engineering, Stanford University.

Cambridge Filter Corporation, 2006. *Cambridge Filter Equipment Catalog.* [Online] Available at: www.cambridgefilterusa.com/Nimages/Cambridge%20Filter%20Catalog%202006.pdf[Accessed 3 July 2016].

CIBSE, 2007. *CIBSE Guide C: Reference Data.* London: CIBSE Publications.

CSIR, 2011. *Climate Risk and Vulnerability: A Handbook for Southern Africa.* Pretoria, South Africa: Council for Scientific and Industrial Research.

da Cunha, I., 2010. *Refrigeration Systems: Energy Efficient Reference Guide,* s.l.: Ceati International.

Department of Environmental Affairs RSA, 2013. *Climate Trends and Scenarios For South Africa: LTAS Phase 1 Technical Report (no. 1 of 6).* s.l.:s.n.

Domanksi, A., 1995. *Theoretical Evaluation of the Vapour Compression Cycle With a Liquid-Line/Suction-Line Heat Exchanger, Economizer, and Ejector,* s.l.: United States Department of Commerce; National Instiute of Standards and Technology .

Ethekwini Municipality, 2015. *Electricity Tariffs 2015 - 2016.* [Online] Available at: http://www.durban.gov.za

Ethekwini Water and Sanitation, 2015. *Annexure "A" - Water Tariffs 2015 / 2016.* [Online]
Available at:
http://www.durban.gov.za/Resource_Centre/Services_Tariffs/Water%20Tariffs/Water%20Tariffs%202015%20-%202016.pdf

Filt Air Ltd., 2014. *Filt AIR Ltd. Filters & Products.* [Online] Available at: http://www.filtair.com/hepaulpafilters/ [Accessed 19 June 2016].

MacKellar, N., New, M. & Jack, C., 2014. Observed and Modelled Trends in Rainfall and Temperature for South Africa: 1960–2010. *South African Journal of Science,* July, 110(7/8), pp. 1 -15.

Matsunaga, K., 2002. *Comparison of Environmental Impacts and Physical Properties of Refrigerants,* s.l.: Earch Engineering Centre of Columbia University.

Niewenhuis, B., Shepperly, C., VanBeek, R. & VanKooten, E., 2012. Project Proposal and Feasibility Study: Atmospheric Water Generator - Water From Air. *Calvin College,* pp. 7 - 15.

Paranjpey, R., 2003. Cooling Cools - Understanding the factors that influence their design and selection. *Air Conditioning and Refrigeration Journal,* pp. 2-10.

Reddy, K., Reddy, M., Venkataswami, A. & Yohan, M., 2013. Improving of Energy Efficiency Ratio of Refrigerant Compressor. *International Journal of Scientific & Technology Research,* May, 2(5), pp. 34 - 40.

South African Statistics, 2005. South African Statistics 2004/05. pp. 22 - 25.